High-Power Green Laser Sources

Alexander Hein

To access the green spectral range for display applications, high-power optically pumped semiconductor disk lasers (OPSDLs) in combination with second-harmonic generation have been realized. A frequency-doubled output exceeding 9.5 W is achieved at a wavelength of 520 nm. The wavelength of these devices can be tuned over a rather broad range of more than 20 nm in the second-harmonic regime. In this article, operation characteristics and limiting mechanisms of OPSDLs are discussed.

1. Introduction

One of the driving applications for green emitters are display technologies. Gallium nitride (GaN) based direct green laser diodes with continuous-wave (CW) output powers above 100 mW at wavelengths up to 532.1 nm were already reported by Sumitomo Electric and Sony [1]. At lower power levels, wavelengths of up to 536.6 nm have been realized which are closer to the peak of human visual sensitivity at 550 nm. These small-power and low-coherence devices are predestined for pico-projector applications, where high output powers are not needed and easy despeckling is required. However, especially for cinema projection which currently relies on xenon arc lamps, there is an occurring need for high-power laser systems. Well established frequency-doubled solid-state laser systems like Nd:YAG or Nd:YVO_4 are struggling with highly demanding cinema requirements and are difficult to despeckle, whereas a Nd:YLF frequency-doubled system from Laser Light Engines Inc. with optical outputs of 30 and 50 W (Q-switched) meets the requirements since it can be utilized in such a way that the output is despeckled [2]. High-power frequency-doubled OPSDLs are other promising candidates for cinema projection because they draw on the advantages of lower coherence for despeckling and unmatched wavelength tailoring to produce any desired gamut. Additionally, similar to solid-state lasers, the small fiber-coupling losses in these high-beam-quality systems may enable off-board illumination when required.

2. OPSDL Structure and Thermal Management

A more detailed description of the layer structure, design strategy, and preliminary characterization measurements such as photoluminescence and reflectivity spectra for these devices were presented in [3]. The semiconductor layer structure with its key elements is depicted in Fig. 1. To achieve high optical outputs with these devices, proper heat removal is required in order to keep the temperature inside the active region with the quantum wells (QWs) low because of thermal leakage and carrier spill-over for structures

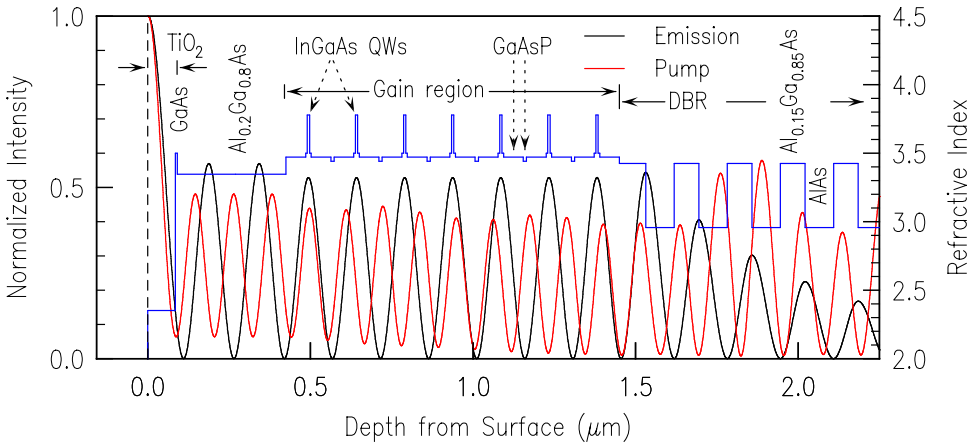

Fig. 1: Refractive index representation of the semiconductor layer structure, complemented by a dielectric anti-reflection TiO_2 surface coating on top. Gain is provided by 7 compressively strained InGaAs QWs surrounded by tensile strained GaAsP pump light absorbing barriers. The structure is finalized by a 56 layer distributed bragg reflector (DBR), transparent for the pump wavelength, and a Ti/Au/Pt/Au metalization. The field intensities of the laser emission and the pump light are also plotted.

with reduced barrier height [4]. Since the heat flux in the semiconductor layers is almost completely one-dimensional it is impossible to extract watt-level heat power from typical pump spot sizes of 500–900 µm. Thus, thick heat spreaders with high thermal conductivities have to be employed. This can be implemented using a transparent intra-cavity heat spreader placed on the semiconductor disk surface to bypass the thermal impedance of DBR mirror and substrate, or as a submount adherent to the mirror where the substrate is removed from a bottom-emitter leaving only a foil of 5–7 µm thickness as the actual semiconductor laser disk. Figure 2 shows secondary electron microscope (SEM) images of a mounted bottom-emitting semiconductor disk on a diamond heat spreader before the substrate was removed.

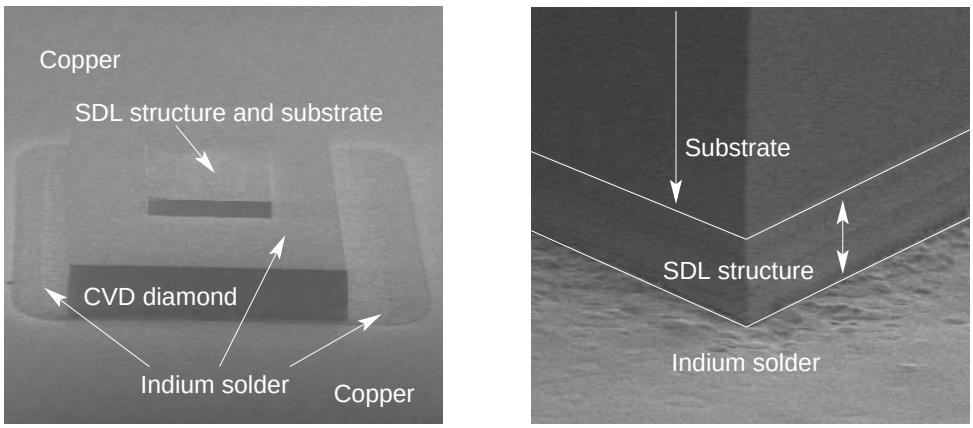

Fig. 2: Semiconductor disk laser with substrate mounted on a CVD diamond heat spreader and a gold-plated copper carrier with a two-step indium evaporation and solder process (left). Enlargement of the disk's edge where the actual device structure can be seen (right).

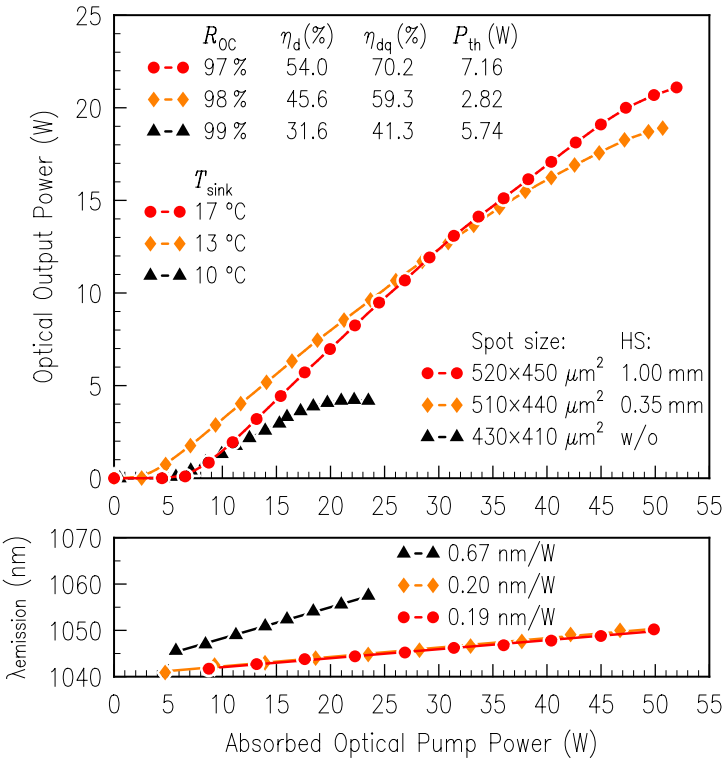

Fig. 3: Comparison of output characteristics for a standard gold-plated copper heat sink device with two devices mounted on CVD diamond heat spreaders with thicknesses of 0.35 and 1.00 mm. The resonator length for all measurements was approximately 140 mm with a mirror radius of curvature of 150 mm, but with output coupler reflectivities R_{OC} chosen for maximum output.

2.1 Heat spreader influence

To efficiently remove the heat from the active region and to increase the output powers of the devices, two different heat spreaders (HS) were investigated. The heat spreader material was chemical vapor deposited (CVD) diamond with thicknesses of 0.35 mm and 1 mm and thermal conductivities of 1800 W/(m · K) and 2000 W/(m · K), respectively. The output characteristics for both devices are depicted in Fig. 3 for a fixed heat-sink temperature. For better comparison and emphasis of the effect, a characteristic of a device without a diamond heat spreader are added in the figure as well. Besides the obvious drastic increase in output power for comparable pump spots and temperatures, the devices with a heat spreader show a much smaller wavelength shift rate per watt of absorbed power. Thermal roll over occurs at an absorbed power of 52 W in case of the thicker heat spreader, while the device with the thinner diamond shows roll-over for a power level of 50 W. The higher output and better slope are attributed to better spreading and heat-transfer characteristics of the thicker heat spreader. However, considering the thickness and accounting for the fact of a 22 % better thermal conductivity, the rather modest increase in output power of 11 % appears to be too small. Since two soldering steps are necessary, fluctuations during these may be an explanation for the only small increase in performance. However, since the point of thermal roll-over is very similar,

the explanation is unsatisfactory and the limit is rather set by the cooling circuit of the system. When the cooling capacity is high enough, output powers in excess of 100 W can be generated by the excitation of larger areas and the use of thicker heat spreaders [5].

2.2 Temperature influence

As reported in [6], changes in the power characteristics with temperature can be used to extract some properties of the OPSDLs. Optical output powers at different heat-sink temperatures are depicted in Fig. 4. The heat-sink temperature was increased from 20 °C to 90 °C in steps of 10 °C, while the output power was recorded until the rollover point. Any other parameters such as cavity length, pump spot size, etc., were kept constant. The maximum extracted output power at 20 °C was 21.5 W and gradually dropped to 3.5 W for a heat-sink temperature of 90 °C. Measurements at higher operation temperature were not performed since the thermoelectric Peltier cooler used for temperature stabilization had a maximum specification of 100 °C. Taking the dissipated heat power, which is given by the relation

$$P_{\mathrm{diss}} = P_{\mathrm{abs}} - P_{\mathrm{out}}, \tag{1}$$

where P_{abs} is the absorbed power and P_{out} is the optical output power, as a function of the respective heat-sink temperature, essential temperature characteristics can be derived as indicated in the left part of Fig. 5. By applying a linear fit to the data points at rollover, the internal shut-off temperature can be extracted from the intersection with the abscissa. For levels above 50 W of absorbed pump power, heat-sink temperatures of 20 °C and 30 °C could not be maintained, so the linear fit only accounts for heat-sink temperatures above 30 °C. For our devices, the roll-over temperature is determined to 145 °C. From the slope it is evident, that, in order to dissipate an additional watt of heat at rollover, approximately a 3 °C lower heat-sink temperature is required. Accounting for a quadratic increase of the threshold pump power, which is included in the dissipated heat term, and for a linear drop in slope efficiency with increasing heat-sink temperature as indicated in the right part of Fig. 5, watt-level operation should be possible at even 110 °C.

At 120 °C, the required threshold power is already higher than the maximum possible

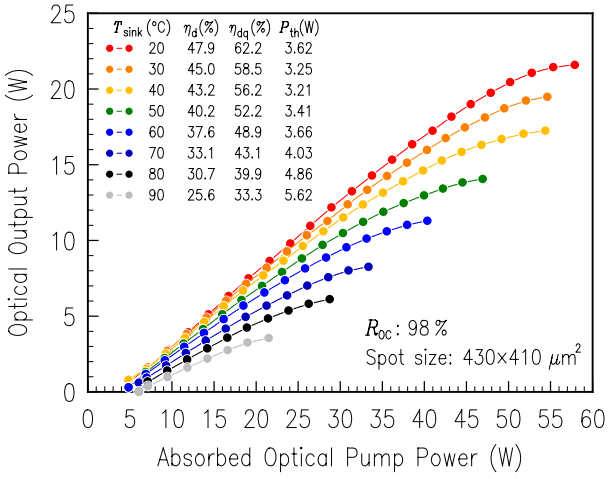

Fig. 4: Output power characteristics for a device with a 1 mm-thick diamond heat spreader up to thermal rollover for heat-sink temperatures T_{sink} from 20 °C to 90 °C. The behavior of slope efficiency η_{d}, differential quantum efficiency η_{dq}, and threshold pump power P_{th} are listed in the legend.

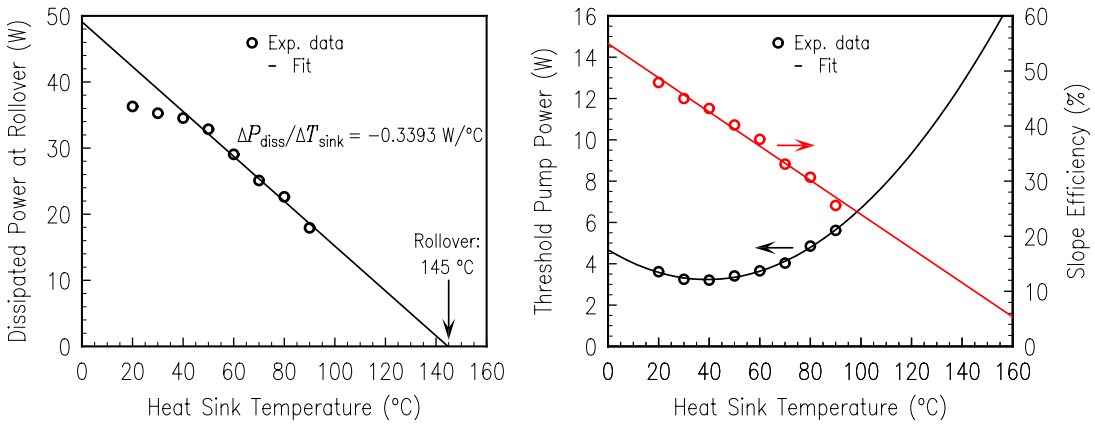

Fig. 5: Dissipated heat power at thermal rollover in dependence of the heat-sink temperature (left). Threshold pump power and slope efficiency vs. heat-sink temperature (right).

heat dissipation at roll-over, so the absolute maximum operating temperature should be around 116–119 °C. It should be noted that the sensor used is specified with an accuracy of ±1 °C. Considering the deviations of the dissipated power at rollover from the linear regression for heat-sink temperatures of 20 °C and 30 °C, it is plausible that the cooling capacity was insufficient and underlines the described heat-sink temperature increase at high pump levels. Proper backside heat dissipation of the thermoelectric cooler or larger dimensioning should lead to higher dissipated heat levels and subsequently higher optical outputs.

3. Green Output

Compared to the results reported in [7], the cavity was modified in order to yield one main output of the second-harmonic (SH) emission through the folding mirror as indicated in Fig. 6, with specified reflectivities for the fundamental and second-harmonic of 99.99 % and < 2 %, respectively. The minor frequency-doubled output from the end mirror was used to monitor and record the emitted wavelength. Polarization and wavelength were controlled via a 4 mm thick birefringent filter (BRF) located in the longer cavity arm. Results obtained with the cavity configuration as pictured in Fig. 6 are summarized in Fig. 7. The second-harmonic output for all three wavelengths was mainly limited by an increase of the heat-sink temperature at pump power levels of 45 W and above. The two curves for the shorter wavelengths yield clearly better output and efficiency characteristics. However, the increasing internal temperature gradually favors the emission at the longer wavelength which explains why at maximum output the curve shows no behavior of a decreasing slope compared to the shorter wavelengths. This is also seen in the steadily rising conversion efficiency of that particular curve. Throughout all measurements, the output was extremely stable, attributed to temperature stabilization of the nonlinear crystal, which was not yet applied in [3]. It was observed that the crystal temperature is steadily rising as long as the input power is increased, thus, changing the phase matching conditions [8]. Adaptation of the crystal angle is then necessary to regain a phase-matched condition.

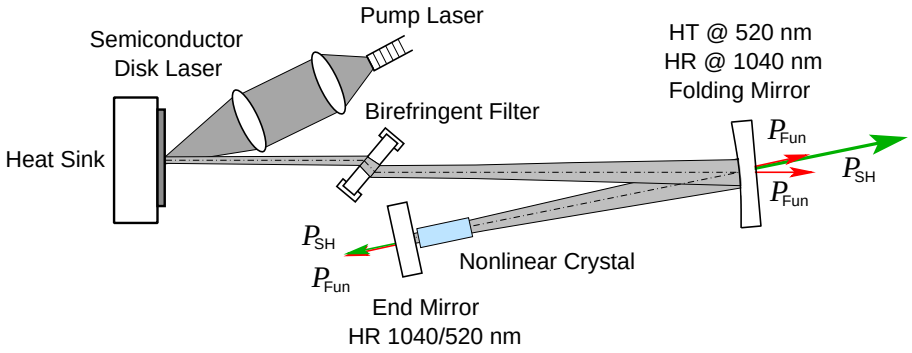

Fig. 6: Folded resonator configuration with highly reflective single (HR/HT) - and double-band (HR/HR) external mirrors enabling a main high-power output of the frequency-converted radiation.

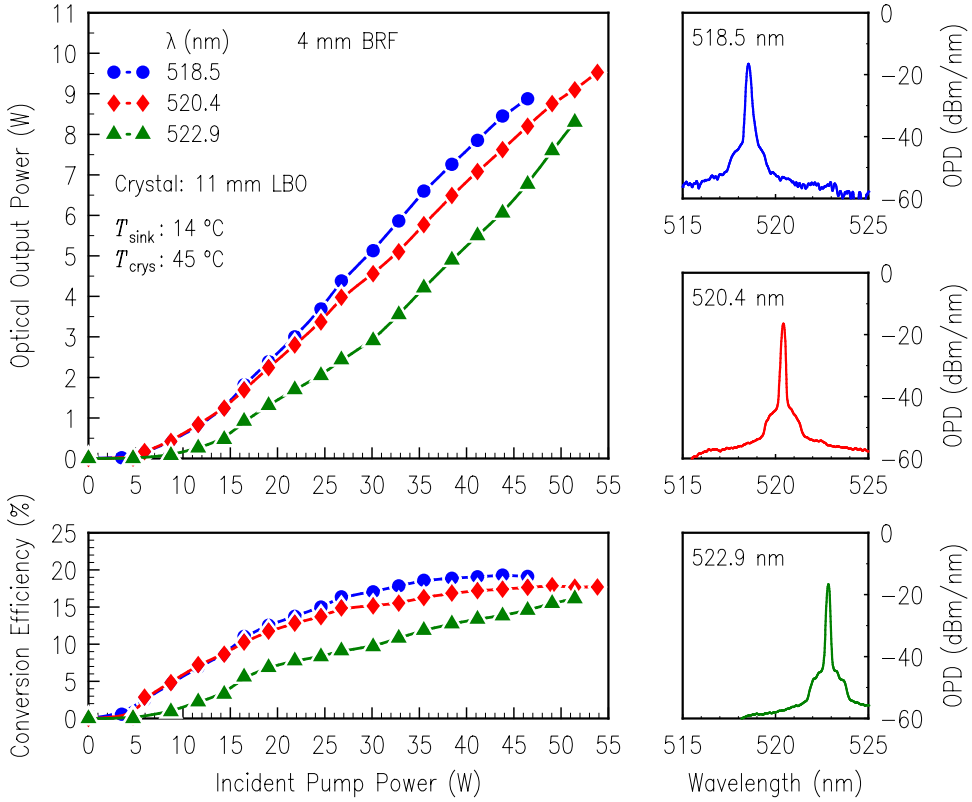

Fig. 7: Second-harmonic output powers and conversion efficiencies for different emission wavelengths. The output powers were generated at a heat-sink temperature of 14 °C, while the temperature of the 11 mm lithium triborate (LBO) crystal was stabilized at 45 °C. Tuning to the respective wavelengths was achieved by rotation of the birefringent filter.

Further improvements to achieve higher efficiencies would require to suppress the rather high losses with a perpendicular polarization caused by the birefringent filter as observed in [9]. Since SDLs are inherently broad gain devices they are also capable of a rather broad tuning range in the SH regime. In operation, the wavelength was shifted by rotating a 2 mm thick BRF around its optical axis without any other adjustments to the cavity

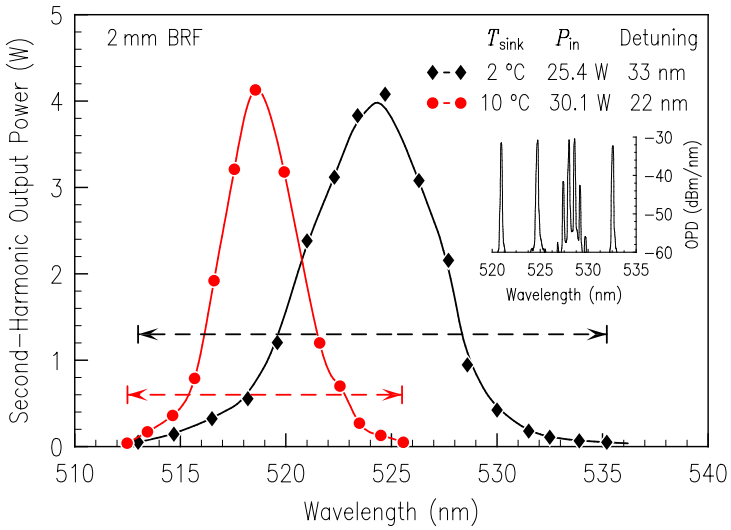

Fig. 8: Output power vs. wavelength in the second-harmonic regime for two devices with different detuning of micro-cavity resonance and QW peak wavelength, and different heat-sink temperatures. The inset shows various recorded spectra during the tuning experiment for the device with the broader tuning range.

or the angular position of the crystal. The measurement was performed on two devices with different detuning (micro-cavity resonance vs. QW peak wavelength) characteristics, as shown in Fig. 8. The obtained tuning bandwidth was 22 nm, ranging from 513 nm to 535 nm for a device with a determined detuning of 20 nm at room temperature. At these boundary values an optical output of roughly 60 mW was measured. A maximum power of 4.1 W was obtained at 524.7 nm. The full-width-at-half-maximum (FWHM) bandwidth with 2 W of SH power is 7 nm. For the second device it is a 13 nm bandwidth for a similarly high optical output at the optimum wavelength. Devices with a smaller detuning naturally yield a narrower tuning range. For certain wavelengths there were multiple peaks indicating parasitic etalon effects, as provided in the inset of the figure, but these could be eliminated by smaller adjustments to the cavity. The origin of these parasitics is not fully understood. The shortest possible wavelength around 513 nm for both devices originates from the fact of a wafer-position-independent QW peak wavelength and the support of the lower heat-sink temperature for the device with the larger detuning. The longest wavelength is simply governed by the micro-cavity resonance, which is red-shifted by 12 nm for the large detuning device.

4. Conclusion

In this work, efficient high-power frequency-doubled semiconductor disk lasers have been realized. High-power operation in the fundamental regime of more than 20 W was achieved with an elaborately designed semiconductor structure and the implementation of a CVD diamond heat spreader. High-temperature operation of the devices up to 110 °C seems possible regarding the extrapolation of the experimental results. In the second-harmonic regime an output power close to 10 W (9.5 W) has been achieved at 520 nm. The tuning

range of the devices under test is as wide as 22 nm for the green output, depending on the detuning properties and operating temperatures.

Acknowledgment

The assistance of Susanne Menzel and Rudolf Rösch with growth and device processing as well as of Andreas Ziegler and Markus Rampp with various measurements is gratefully acknowledged.

References

[1] J. Hecht, "Nitride diode sources grow greener", *Laser Focus World*, pp. 32–35, Nov. 2012.

[2] B. Beck and I. Lee, "High-power RGB laser engine powers digital projection displays", *Laser Focus World*, pp. 29–31, Nov. 2012.

[3] A. Hein and S. Menzel, "Design and characterization of high-power optically pumped green-emitting semiconductor disk lasers using second-harmonic generation", *Annual Report 2011*, pp. 69–76. Ulm University, Institute of Optoelectronics.

[4] A.P. Ongstad, D.J. Gallant, and G.C. Dente, "Carrier lifetime saturation in InGaAs single quantum wells", *Appl. Phys. Lett.*, vol. 20, pp. 2730–2732, 1995.

[5] B. Heinen, T.-L. Wang, M. Sparenberg, A. Weber, B. Kunert, J. Hader, S.W. Koch, J.V. Moloney, M. Koch, and W. Stolz, "106 W continuous wave output power from a vertical-external-cavity surface-emitting laser", *Electron. Lett.*, vol. 48, no. 9, pp. 516–517, 2012.

[6] B. Heinen, F. Zhang, M. Sparenberg, B. Kunert, M. Koch, and W. Stolz, "On the measurement of the thermal resistance of vertical-external-cavity surface-emitting lasers (VECSEL)", *IEEE J. Quantum. Electron.*, vol. 48, no. 7 pp. 934–940, 2012.

[7] A. Hein, S. Menzel, and P. Unger, "High-power high-efficiency optically pumped semiconductor disk lasers in the green spectral region with a broad tuning range", *Appl. Phys. Lett.*, vol. 101, pp. 111109-1–4, 2012.

[8] A. Ziegler, *Experimentelle Untersuchungen zur resonatorinternen Frequenzverdopplung mit hoher Ausgangsleistung im grünen Spektralbereich*. Bachelor Thesis, Ulm University, Ulm, Germany, 2012.

[9] M. Rampp, *Charakterisierung von optisch gepumpten Halbleiterscheibenlasern mittels verschiedener Resonatorkonfigurationen, sowie polarisations- und frequenzselektiver Elemente*. Bachelor Thesis, Ulm University, Ulm, Germany, 2012.